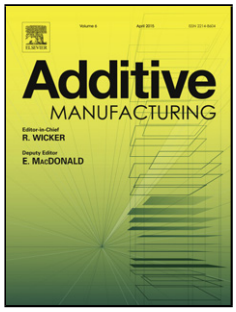

Title: Improving the filament weld-strength of Fused Filament Fabrication products through improved interdiffusion

Authors: Yee Song Ko, Denis Herrmann, Oliver Tolar, Wilfried J. Elspass, Christof Brändli

PII: S2214-8604(19)30320-3
DOI: https://doi.org/10.1016/j.addma.2019.100815
Article Number: 100815

Reference: ADDMA 100815

To appear in:

Received date: 18 March 2019
Revised date: 15 May 2019
Accepted date: 28 July 2019

Please cite this article as: Song Ko Y, Herrmann D, Tolar O, Elspass WJ, Brändli C, Improving the filament weld-strength of Fused Filament Fabrication products through improved interdiffusion, *Additive Manufacturing* (2019), https://doi.org/10.1016/j.addma.2019.100815

Improving the filament weld-strength of Fused Filament Fabrication products through improved interdiffusion

Yee Song Ko[a], Denis Herrmann[b], Oliver Tolar[b], Wilfried J. Elspass[b], Christof Brändli[a*] brae@zhaw.ch

[a]Zurich University of Applied Sciences, Institute of Materials and Process Engineering, Laboratory of Adhesives and Polymer Materials, Technikumstrasse 9, 8401 Winterthur, Switzerland

[b]Zurich University of Applied Sciences, Institute of Mechatronic Systems, Technikumstrasse 9, 8401 Winterthur, Switzerland

*Corresponding author.

Graphical Abstract

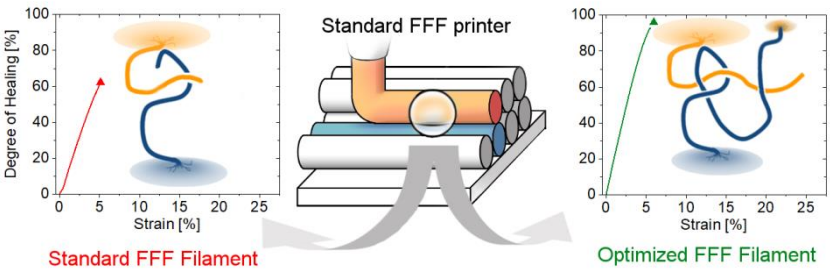

Abstract

Fused Filament Fabrication (FFF) is a popular additive manufacturing technique where molten polymer filament is applied in a raster pattern, layer by layer, to obtain the work piece. A necessary consequence of this method is a pronounced mechanical anisotropy of the product; the interface between the filaments is weaker compared to the filament itself. The strength of this interface is governed by the reptation theory which postulates a more efficient interpenetration of polymeric surfaces with decreasing polymer viscosity. This relationship was utilized in this work to modify a polycarbonate-acrylonitrile butadiene styrene polymer blend to produce FFF work pieces with less mechanical anisotropy, independent of printer settings. The tensile strength ratio of the printed interface to bulk tensile strength could be increased from 41% to 95%. Though the absolute bulk tensile strength decreases slightly, this method presents an easy and effective way to address the mechanical problems inherent in the FFF-method.

Keywords: Fused Filament Fabrication; Welding time; Interfacial adhesion; Plasticizer; PC-ABS

1. Introduction

Since its inception, additive manufacturing has been successfully applied to various prototyping challenges and is nowadays a mainstay in many concept stages of product design, as well as being a viable production method by itself [1–3]. Polymer-based additive manufacturing methods have proven to be very popular due to their ability to produce complex geometric shapes, the ease with which they can be switched to new shapes and their low adoption and material costs [4–6]. Fused filament fabrication (FFF), also called material extrusion based on additive manufacturing [7], is one of the polymer-based methods in which a thermoplastic filament is fed to a heated nozzle that deposits the hot material in layers of predetermined raster patterns on top of a print-bed (see Figure 1) [7,8]. While applications for this technique are being developed rapidly, for example producing parts in space-faring structures [9], or unmanned aerial vehicles [10], great care has to be placed in designing the printing sequence due to considerable mechanical anisotropy. Parts produced by FFF show lesser mechanical strength against the print direction and in the direction of the stacked layers compared to the bulk material; the interface between the raster-lines are a weak point of failure [11]. Some aspects of this can be addressed by optimizing the printing process, such as raster pattern [12], nozzle temperature [13], print speed [14] or material infill [15]. However, all these parameters ultimately have to take into account the base material properties. The aim of this paper is to qualify the relevant material properties and present optimization methods independent of the printer settings.

This problem, the adequate diffusion of polymer molecules across two heated polymer surfaces, has been extensively studied in the context of polymer welding and polymer healing [16–19]. An ideal situation is described when two polymeric interfaces are heated to temperatures above their glass transition temperature T_g, or melting temperature T_m, and brought into intimate contact. The developing interfacial bond strength, σ, depends on the number of polymer chains and the distance they move beyond the initial interface into the other side, schematically illustrated in Figure 2. The process continues until the molecular structure of the interface is indistinguishable from the bulk at the reptation time t_r, where this interpenetration distance, χ, is at its maximum, χ_∞. χ can be predicted using the reptation theory by De Gennes and Edwards [20,21],which describes the motion of polymer chains in bulk materials and concentrated solutions. To describe the healing process, a degree of healing D_h is introduced as the ratio of the developing interfacial bond strength σ and the bulk tensile strength σ_∞ [22]:

$$D_h(t) = \frac{\sigma}{\sigma_\infty} = \frac{\chi}{\chi_\infty} = \left(\frac{l}{L}\right)^{1/2} = \left(\frac{t}{t_r}\right)^{1/4} \quad (1)$$

with l and L the momentary and maximum interpenetrated polymer chain length and t the time passed since interdiffusion started. It has been pointed out, that for very long polymer chains where the molecular weight $M >> M_c$, M_c being the critical entanglement molecular weight, χ does not have to reach χ_∞ to achieve its maximum bond strength σ_∞ [23,24]. This is the case for nearly all engineering thermoplastics and consequently σ_∞ is reached at t_w, the welding time, at which point χ and l have the values χ_w and L_w respectively, giving

$$D_h(t) = \frac{\sigma}{\sigma_\infty} = \frac{\chi}{\chi_w} = \left(\frac{l}{L_w}\right)^{1/2} = \left(\frac{t}{t_w}\right)^{1/4} \quad (2)$$

where t_w can be empirically fitted to an Arrhenius relation[25]

$$t_w = A \exp\left[\frac{E}{R}\left(\frac{1}{T} - \frac{1}{T_{ref}}\right)\right] \quad (3)$$

with A a fitting constant, E an activation energy, T_{ref} a reference temperature, and R the universal gas constant. This model provides a convenient method to quantify the weld quality, and therefore the FFF-printing quality, of a material at set print parameters. Healing experiments in which t_w is determined are, while not simple, quite straightforward: two interfaces are brought into intimate contact and heated to a set temperature for a set time. D_h can then be determined by pulling them apart again and comparing the weld tensile strength σ to the bulk tensile strength σ_∞. t_w can be determined by a linear fit of D_h against $t^{(1/4)}$ and noting that $D_h(t_w) = 1$. Doing this at multiple temperatures allows the temperature dependence of t_w to be fitted with equation 3. There are a variety of methods available in the literature to probe D_h, for example by producing lap-shear samples [25,26], tensile samples by direct joining [27] or even plate on plate samples to be measured with a rheometer [28]. Healing experiments with which the Arrhenius expression in Equation 3 are obtained are the only method to obtain a direct measure of the mechanical properties of the welding interface, solely dependent on the material properties.

Equation 2 also provides a path to improved FFF-weld properties, independent of print parameters: l has been shown [29] to proceed with:

$$l \propto (Dt)^{-1/2} \quad (4)$$

D being the self-diffusion coefficient of the polymer chain along its diffusion path. While it can be intuitively understood, that improving the polymer/polymer interface is tied to making the polymer more mobile, the dependence of t_w on polymer self-diffusion justifies various approaches to influence the weld quality. For example, D is famously dependent on the molecular weight M according to [30,31]

$$D \propto M^{-2} \quad (5)$$

It therefore would be quite elegant to alter M to obtain better interpenetration and therefore printing results. Formula 4 shows another, easier, approach, which relies on increasing D for higher χ values. D is inversely proportional to the polymer melt viscosity η *via* the local friction factor ζ, specifically [32–34]

$$\eta = F\,\zeta \quad (6)$$

$$D = \left(\frac{kT}{\zeta}\right) G \propto \frac{1}{\eta} \quad (7)$$

where k is the Boltzmann constant and F and G are functions of the molecular structures. It follows, that another effective method to modify the welding properties of polymers would be to manipulate its viscosity. Plasticizers are frequently used to influence the viscosity of polymer melts, without, or only marginally altering the mechanical properties of the bulk product [35,36]. They are widely applied to fine-tune industrial polymer products, mainly because of the ease of implementation. They are varied in type and effect but generally act by interposing themselves between polymer chains, and thus giving them more room to move [36,37]. In fact, typical FFF-filaments already seem to have drastically lower melt viscosity, compared to pellets destined for more traditional production methods, such as injection molding or extrusion, of the same base material [38]. On the flip side, plasticizers can also affect other properties, T_g, Young's modulus and tensile strength among others. The lower viscosity can also affect the FFF-part-quality by lowering the form-stability of the printed part. These effects will have to be monitored.

This approach was chosen here and a series of increasing plasticizer concentrations were added to a base polymer to determine the effect on the interpenetration properties themselves *via* healing experiments, but also on interfaces in real FFF-printed parts. To make these experiments relevant for commercial FFF applications, the common engineering thermoplastic blend polycarbonate-acrylonitrile butadiene styrene (PC-ABS) was chosen as the base polymer. Due to the ubiquity of PC-ABS, several effective, viscosity-lowering plasticizers are already known. Triphenyl phosphate (TPP) is often used to improve the flow properties of PC-ABS[36].

The methodology of this paper can thus be stated as follows: t_w at set temperatures, for samples with different plasticizer contents were determined and used to obtain the Arrhenius expression in Equation 3 which yields $t_w(T)$. These expressions can be used to compare the weld-quality of these plasticizer-containing samples and, using the same materials, FFF tensile test bars were produced to validate the results. The printing pattern can significantly influence the maximum achievable tensile strength of these bars [39], which is why samples were printed using three different patterns, as seen in Figure 3. These are samples printed along the long edge (l-samples), along the short edge (s-samples) and standing (st-samples), in which the printed bulk structure, the interface within the print layers and the interface between the print layers respectively are primarily tested. Doing so will show, that $t_w(T)$ can be easily manipulated by modifying polymers with plasticizers, that $t_w(T)$ is a good parameter to compare polymer print quality, and that $t_w(T)$ can be used to predict the mechanical properties of a FFF-printed product. The melt flow index (MFI) was measured to compare the viscosity changes effected by the TPP qualitatively. It would be more elegant to measure melt viscosity η directly. As none of the models used in this manuscript uses η, MFI was sufficient for comparison.

Having access to t_w (T) of a material opens the possibility of predicting the interfacial adhesion in printed products. Costa *et al.* have already developed an algorithm with which the temperature evolution and D_h can be predicted by an iterative method [40]. The algorithm aims to calculate the thermal evolution of each segment of the work piece with each iteration, while also calculating the incremental D_h achieved at the current iteration using formula 2. In this manner the incremental D_h of each segment can be added up and the sums averaged to obtain a final D_h. The algorithm does take into account the actual contact area of the filaments, but only in the heat-transfer calculations. D_h is therefore not corrected for voids. In the initial application of the algorithm, the D_h-calculation was limited to the test direction of s-samples to facilitate implementation, though nothing fundamentally constrains its viability towards other test directions or geometries.

2. Materials and methods

2.1. Materials

PC-ABS resin, Cycoloy CX7211 from Sabic, was kindly provided by Stüdli Plast AG. TPP of 99% purity was purchased from ACROS organics. Three material configurations were tested; one being the neat PC-ABS resin (S0), as well as two further PC-ABS variations with 5 wt% (S5) and 10 wt% (S10) plasticiser. The blends, S5 and S10, were produced by extruding a mixture of PC-ABS and plasticiser with a Collin Teach-Line ZK25T through a circular nozzle, 3mm in diameter, and pelletizing the homogeneous extrudate. The three heating zones of the extruder, from feed to die, were heated to 205°C, 205°C and 207°C, while the die was kept at 210°C. The feed rate was 1 kg h^{-1} and the screw speed was 20 rpm.

2.2. Injection molded samples for tensile- and healing experiments

Bar-shaped tensile testing samples with dimensions of 4 mm × 10 mm × 80 mm were injection molded with a Boy XS injection molding machine. The temperature in the injection unit was 220°C in all temperature zones, while the mold was heated to 70°C. Injection speed was a constant 5 mm s^{-1} and injection pressure was kept at 90 bar and then holding pressure was linearly increased to 200 bar in 5 seconds. The bars were further used to obtain healing experiment samples with more manageable dimensions. The bars were heated to 220°C and compressed between two plane metal plates to a thickness of 1 mm using a Collin P200PV hot press at 5 bar in 3 minutes, which were finally cut into 4.75 mm broad strips. Compression at 220°C ensured final samples free from inner stresses, as evidenced by the samples retaining their dimensions when slowly heated again. Healing experiments were carried out by first cutting the sample strips in half and polishing the cut surface with 800/2400 grit sandpaper. Both cut surfaces were then brought into contact and under slight pressure were fastened in place with Flashbreaker adhesive tape (produced by Airtech international inc.). The tape was needed to prevent the samples from moving during transport and measurement. A schematic representation of the sample preparation process can be seen in Figure 4.

The joined samples were then placed in a preheated Collin P200PV, which was immediately closed to 1.1 mm, which is 40 µm more than the sample thickness plus the tape, set by metal spacers. The temperature was kept constant during each test and was well above the T_g of the material, which can be seen in Table 1. After the testing time, the samples were removed and tested as tensile samples. Various combinations of temperatures and testing times were screened according to Table 2. The tensile strength of the cut and treated samples, normalized by the tensile strength of the untreated samples, corresponded to D_h at the set temperature and testing time. The separation of the samples and the hot metal surface by a sole piece of tape ensured a near immediate heating of the sample to the testing temperature and a good approximation of the testing time to the actual treatment time at the testing temperature. The tape itself is thermally stable up to 230°C, as shown in figure 1 of the supporting information (SI) and could always be removed residue-free from the sample surface. At least five samples were prepared for each temperature and testing time combination.

2.3. FFF-printed samples

The pellets were extruded with a Extrudex ED.N20.25D to produce filaments, spooled with a Collin belt take-off BAW130 with horizontal winder WR650, making it possible to process them using FFF. The extrusion parameters can be seen in Table 3 and the filament diameter was measured with callipers every few meters. The average diameter was 1.6 mm with 1.5 mm and 1.7 mm being the minimum and maximum

measured diameters. The printer was custom built and is described in the SI. Tensile test samples were FFF-printed from all three materials, using three different printing patterns: l-samples, s-samples and st-samples (Figure 3). The filament was extruded from a 0.4 mm circular nozzle and the extrusion width was 0.47 mm and the layer height was 0.2 mm, with an extrusion temperature of 260°C. Some pressure was exerted on the filament, owing to the fact that a 0.4 mm diameter filament was compressed to 0.2 mm, though the exact value is not known. The print speed was 2 mms^{-1} and the sample was printed on a printing bed coated with Polyethyleneimine heated to 120°C. The st-samples were printed on Flashbreaker adhesive tape. The sample dimensions were the same as the injection molded samples (4 mm × 10 mm × 80 mm). A degree of healing for FFF-printed samples,

$$D_{h,l} = \frac{\sigma_s}{\sigma_\infty}, D_{h,s} = \frac{\sigma_l}{\sigma_\infty} \text{ and } D_{h,st} = \frac{\sigma_{st}}{\sigma_\infty} \quad (8)$$

can be defined by normalizing the tensile strengths of s-samples (σ_s), l-samples (σ_l) and st-samples (σ_{st}) by the tensile strength of the injection-molded samples (σ_∞) of the corresponding materials. It has to noted, that these D_h are meant to make comparisons among FFF-printed samples easier. Comparisons to the healing experiments are difficult, due to the non-isothermal nature and the voids in the FFF-sample which are intrinsic to the process. Methods addressing this specific question have been developed [41,42], but are outside the scope of this paper.

2.4. Standard methods

MFI of all three samples were determined using a Zwick 4105.01/03 melt flow indexer to assess the impact of the TPP on the melt viscosity. Measurements were carried out according to ISO-1133 [43] at 230°C and with 2.16 kg load. All injection molded-, welding time- and FFF-printed tensile samples, were investigated with a Zwick Z5.0 tensile testing machine. The starting distance between the clamps was 30 mm, with a clamping pressure of five bar and a testing speed of 10 mm min^{-1}. The sample elongation was measured by the crosshead position. Five specimens per sample were tested for all samples. Optical microscopy images were taken on a Keyence VHX-6000 digital microscope with 20x magnification. The fracture surface of all tensile test samples were investigated in this manner. Dynamic scanning calorimetry was carried out in a Netsch DSC 204 F1 Phoenix with a temperature program that heated samples twice form room temperature to 300°C at a rate of 20°C min^{-1}.

2.5. Degree of healing calculations for FFF-samples

The theoretical degree of healing of FFF-printed samples were calculated for all three materials as described in literature,[38] for the geometry of a s-sample. The Matlab code can be seen in the SI. The thermal conductivity of 0.2 W $m^{-1}°C^{-1}$ and the specific heat of 2 J g^{-1} were taken from the PC-ABS datasheet and heat transfer coefficients between adjacent filaments, 70 W $m^{-2}°C^{-1}$, and filament and support, 300 W $m^{-2}°C^{-1}$, are taken from literature [40].

3. Results and Discussion

Initial tensile tests depicted in Figure 5 (curves of the individual specimen can be seen in the SI) of injection-molded bars show lower tensile strengths for samples with higher TPP contents, while at the same time strain at break increases, consistent with expectations. A summary of all tensile testing data together with standard deviations can be found in Table 4. The Young's modulus doesn't seem to change significantly by the addition of TPP, but a decrease of tensile strength of 17% from 62.2 MPa to 51.8 MPa and an increase of strain at break of 73 % from 13.5 to 23.3 % is observed by adding 10% of TPP.

The so measured tensile strengths are used to calculate D_h in the healing experiments according to Equation 1, which were then plotted against $t^{(1/4)}$ in Figure 6. The seemingly linear form of D_h when visualized in this manner, strongly suggests a healing behaviour proportional to $t^{(1/4)}$, as predicted by Equation 2, which also holds true for the TPP-modified materials. A linear least square fit to D_h with a fixed intercept at zero was done for all three materials at each test-temperature. t_w was then approximated by the time at $D_h = 1$, as determined by the fit. The results are tabulated in Table 5 and show that at a given temperature, t_w decreases by roughly an order of magnitude when the TPP content is increased by 5%, meaning that significantly less time is needed to heal samples with high TPP contents. Alternatively, the same t_w can be achieved by increasing the TPP content of 5 % and decreasing the temperature by 5K at the same time. It is even more visible when plotted as in Figure 7. In that figure, interpolations to the print temperature of 260°C show t_ws in the range of milliseconds. Other authors have showed, that it typically takes only a few seconds for the printed filament temperature to drop by as much as 100°C [40,44,45]. It is therefore reasonable to assume, that most mechanical strength is recovered during the first few seconds, or even milliseconds, where the filament temperature corresponds to a low t_w. The data for S5 at 210°C has a significantly higher scatter than other datasets, which is probably due to insufficient sanding of the healing samples. It was nevertheless included here to complement the data of S5. All the data relevant to the healing process is summarized in table 6. A dramatic increase in interface quality of printed parts can therefore be expected by adding TPP or by increasing printing temperature. Concurrently melt flow viscosity decreases, as seen in the significantly higher MFI-values (Table 4), linking the decreased welding times to decreased melt viscosities. At the same time, T_g of also sinks with increased TPP content.

While there was no noticeable difference in the difficulty to print with the different materials (st-samples were difficult to print with all materials), S5 and S10 exhibited markedly rougher exterior finishes, due to the material flowing after being deposited. The relatively high MFI values are responsible for this behaviour, but as the samples were fine, apart from their outside appearance, they were used in all the experiments. FFF-printed tensile specimens were tested, such as seen in Figure 8 (curves of the individual specimen can be seen in the SI), s- and st-samples show improved tensile strengths with increasing TPP content. By adding 10 wt% TPP, a $D_{h,s}$ of 95%, up from 41%, could be achieved (D_h-values can be seen in Table 6). Concurrently $D_{h,st}$ increases even more dramatically from 8% to 45%, though its starting D_h-value is significantly lower. These two samples also show, that both the interface within and between the print layers are improved by adding TPP. Even considering the lower tensile strength of the modified materials, an absolute increase in the interface adhesion was realized. The difference most probably stems from two sources. First, the contact of interfaces within the layers are established relatively fast, as the printer only has to complete a line before turning and contacting the interface with new material. In contrast, the printer has to complete a full layer before the interface is contacted with material again to start the healing process between layers. Secondly, as only the printing bed is heated, st-samples will cool significantly faster the higher the sample is built. Both of these mechanisms lead to a lower temperature of the material being contacted and thus lower $D_{h,st}$. All materials, though, exhibit a brittle failure mode when printed as s- and st-samples, breaking well below the strain at stress maximum λ_m. Simply reaching M_c, the definition of $D_h = 1$, is insufficient to recover the strain

at break values achieved by the bulk material. It has been postulated, that chain lengths in excess of M_c are necessary to facilitate ductile failure in a polymer material.[46]

$D_{h,l}$ remains stable at values above 90%. More importantly, there is significant ductile deformation before failure, with strain at break values similar to injection-molded samples. Interestingly the FFF-printed S0 l-samples show much larger strain at break values compared to their injection-molded counterparts due to the weak inter-layer adhesion deflecting propagating cracks. The similarity of l-samples to injection-molded samples underscores the importance of interfacial adhesion as a weaker point of failure in printed samples.

The positive effect of a less viscous polymer melt can also be seen in the Young's modulus, as demonstrated again in Table 4: the Young's modulus of S0 st-samples Y_{st} is significantly lower than the bulk Young's modulus Y_∞, probably due to the weak interface adhesion lowering the real load bearing surface area. The value becomes comparable to bulk-values in S5 and S10. This is supported by optical microscopy images seen in Figure 9: The fracture surface of S0 st-samples clearly shows, that many of the filaments have not properly fused together during printing, while the fracture surface of st-samples of S5 and S10 samples seem more smeared out, indicating a better fusion of the printing layers. The same is true to a lesser extent for s-samples. In all these cases, the images show clear brittle failure of the samples. Injection molded and l-samples clearly show plastic deformation before failure, the most prominent feature being the necking evident in all samples. Also, increased plastic deformation of the fracture surface itself can be observed in injection molded samples at increasing TPP concentrations. This effect is less pronounced in the l-samples, but there the decreasing average void size can be taken as an indication of the lower print melt viscosity. The Young's modulus of FFF samples are generally lower than their injection molded counterparts, probably again due to a lowering of the load bearing area caused by voids. The one exception is the S0, which has a higher Y_l than Y_∞. The reason for this is the orientation of the polymer chains in the tensile testing direction during printing. The high viscosity during printing of the material renders the chains unable to relax back to a more random conformation. The viscosity during printing in S5 and S10 on the other hand seems to be low enough to allow for the polymer chains to relax, thus lowering their Y_l. Future experiments should aim to retain the tensile strength of the unmodified base material. In the case of PC-ABS, Resorcinol bis(diphenyl phosphate), which is an oligomeric phosphate similar to TPP, is known to modify flow, without influencing the mechanical properties.

The Arrhenius expressions $t_w(T)$ were used to predict the interface adhesion of all three materials using the method mentioned in the introduction and the results can be seen in Table 6. It is immediately apparent that the predictions are generally higher than the obtained $D_{h,s}$ values. One source of error could be incorrect material parameters, leading to inaccurate calculated cooling rates. All three materials use the same parameters listed in the theory section and the $D_{h,s}$ of the most heavily modified material actually agrees best with the calculated value. Materials parameters therefore seem to play a secondary role in this case. Another explanation could be the weakening of the tensile sample by voids formed during the printing process. As viscosity decreases with higher TPP contents, the material flows more readily to fill the voids. When samples with 110% infill were printed, overfilling possible voids, the $D_{h,s}$ of S0 and S5 increase to 65% and 86% respectively. The images in Figure 9 do show voids in the samples and more comprehensive set of images could be used to determine the actual contact area between the filaments. If anything, this shows the need to account for possible production errors in future calculation methods and the necessity to produce void-free parts if the best possible performance is to be achieved.

For the ultimate use case of $t_w(T)$ to predict the strength of a FFF-printed product in all failure modes, or using $t_w(T)$ to prescribe optimal print parameters, a more complete model is needed. Work has been done to address temperature gradients during printing, either by monitoring [44] or by simulation [45], material

wetting during initial contact [47], printing defects [41,42] and effects of melt orientation [48]. The diverse work aimed at weld strenght prediction showcases the complicated nature of this endeavor, though some kind of description of $t_w(T)$ will always be necessary.

4. Conclusions

It has been shown that by adding appropriate amounts of plasticizer to PC-ABS the flow properties of the polymer melt and the interfacial adhesion of FFF-printed parts are considerably improved. The improvement can be explained by the well-known reptation theory, which predicts better polymer interpenetration with improved flow properties. The tensile strength of printed parts can be significantly increased by the addition of 10 wt% of TPP to PC-ABS. Further development is necessary though to achieve the same for strain at break when pulling print layers apart. Because plasticizers are already ubiquitous in the industry, it is the conceivably easiest method to lower the viscosity of FFF-filament and improve the quality of FFF-printed parts. While it harbours the danger of lowering the mechanical properties of the material, know-how and compounds exist to achieve the desired effect with minimal impact for a variety of polymers. MFI can be used to quickly monitor the modifications, while the welding time characteristics in the form of $t_w(T)$ enables a more in-depth comparison of the effect of the modification.

Acknowledgements

This work was partially funded by the Swiss Innovation Agency (Innosuisse). The support from Stüdli Plast AG is greatly acknowledged.

References

[1] T.D. Ngo, A. Kashani, G. Imbalzano, K.T.Q. Nguyen, D. Hui, Additive manufacturing (3D printing): A review of materials, methods, applications and challenges, Compos. Part B Eng. 143 (2018) 172–196. doi:10.1016/j.compositesb.2018.02.012.

[2] D.R. Eyers, A.T. Potter, Industrial Additive Manufacturing: A manufacturing systems perspective, Comput. Ind. 92–93 (2017) 208–218. doi:10.1016/j.compind.2017.08.002.

[3] J.-P. Kruth, M.C. Leu, T. Nakagawa, Progress in Additive Manufacturing and Rapid Prototyping, CIRP Ann. 47 (1998) 525–540. doi:10.1016/S0007-8506(07)63240-5.

[4] S. Singh, S. Ramakrishna, R. Singh, Material issues in additive manufacturing: A review, J. Manuf. Process. 25 (2017) 185–200. doi:10.1016/j.jmapro.2016.11.006.

[5] S. Berretta, R. Davies, Y.T. Shyng, Y. Wang, O. Ghita, Fused Deposition Modelling of high temperature polymers: Exploring CNT PEEK composites, Polym. Test. 63 (2017) 251–262. doi:10.1016/j.polymertesting.2017.08.024.

[6] S.C. Ligon, R. Liska, J. Stampfl, M. Gurr, R. Mülhaupt, Polymers for 3D Printing and Customized Additive Manufacturing, Chem. Rev. 117 (2017) 10212–10290. doi:10.1021/acs.chemrev.7b00074.

[7] ASTM 52903, Additive manufacturing - Standard specification for material extrusion based additive manufacturing of plastic materials, ASTM Standards.

[8] R. Singh, H.K. Garg, Fused Deposition Modeling – A State of Art Review and Future Applications, in: Ref. Modul. Mater. Sci. Mater. Eng., Elsevier, 2016. doi:10.1016/B978-0-12-803581-8.04037-6.

[9] D. Turbiner, Phased antenna array for global navigation satellite system signals, US9190724B2, 2015.

[10] H. Klippstein, A. Diaz De Cerio Sanchez, H. Hassanin, Y. Zweiri, L. Seneviratne, Fused Deposition Modeling for Unmanned Aerial Vehicles (UAVs): A Review, Adv. Eng. Mater. 20 (2018) 1–17. doi:10.1002/adem.201700552.

[11] C. Bellehumeur, L. Li, Q. Sun, P. Gu, Modeling of Bond Formation Between Polymer Filaments in the Fused Deposition Modeling Process, J. Manuf. Process. 6 (2004) 170–178. doi:10.1016/S1526-6125(04)70071-7.

[12] M.S. Islam, P. Prabhakar, Interlaminar strengthening of multidirectional laminates using polymer additive manufacturing, Mater. Des. 133 (2017) 332–339. doi:10.1016/j.matdes.2017.07.038.

[13] X. Deng, Z. Zeng, B. Peng, S. Yan, W. Ke, Mechanical Properties Optimization of Poly-Ether-Ether-Ketone via Fused Deposition Modeling, Materials (Basel). 11 (2018) 216. doi:10.3390/ma11020216.

[14] K.G.J. Christiyan, U. Chandrasekhar, K. Venkateswarlu, A study on the influence of process parameters on the Mechanical Properties of 3D printed ABS composite, IOP Conf. Ser. Mater. Sci. Eng. 114 (2016) 012109. doi:10.1088/1757-899X/114/1/012109.

[15] M. Fernandez-Vicente, W. Calle, S. Ferrandiz, A. Conejero, Effect of Infill Parameters on Tensile Mechanical Behavior in Desktop 3D Printing, 3D Print. Addit. Manuf. 3 (2016) 183–192. doi:10.1089/3dp.2015.0036.

[16] M.J. Shim, S.W. Kim, Characteristics of polymer welding by healing process, Mater. Chem. Phys. 48 (1997) 90–93. doi:10.1016/S0254-0584(97)80084-3.

[17] A. Aradian, E. Raphaël, P.-G. de Gennes, Strengthening of a Polymer Interface: Interdiffusion and Cross-Linking, Macromolecules. 33 (2000) 9444–9451. doi:10.1021/ma0010581.

[18] O.A. Ezekoye, C.D. Lowman, M.T. Fahey, A.G. Hulme-Lowe, Polymer weld strength predictions using a thermal and polymer chain diffusion analysis, Polym. Eng. Sci. 38 (1998) 976–991. doi:10.1002/pen.10266.

[19] Y.Q. Xue, T.A. Tervoort, P.J. Lemstra, Welding Behavior of Semicrystalline Polymers. 1. The Effect of Nonequilibrium Chain Conformations on Autoadhesion of UHMWPE, Macromolecules. 31 (1998) 3075–3080. doi:10.1021/ma970544u.

[20] P.G. de Gennes, Reptation of a Polymer Chain in the Presence of Fixed Obstacles, J. Chem. Phys. 55 (1971) 572–579. doi:10.1063/1.1675789.

[21] S. Edwards, The statistical mechanics of polymerized material, Proc. Phys. Soc. 92 (1967) 9. http://iopscience.iop.org/article/10.1088/0370-1328/92/1/303.

[22] S. Prager, M. Tirrell, The healing process at polymer–polymer interfaces, J. Chem. Phys. 75 (1981) 5194–5198. doi:10.1063/1.441871.

[23] R.P. Wool, B.-L. Yuan, O.J. McGarel, Welding of polymer interfaces, Polym. Eng. Sci. 29 (1989) 1340–1367. doi:10.1002/pen.760291906.

[24] R.P. Wool, K.M. O'Connor, A theory crack healing in polymers, J. Appl. Phys. 52 (1981) 5953–5963. doi:10.1063/1.328526.

[25] F. Yang, R. Pitchumani, Healing of thermoplastic polymers at an interface under nonisothermal conditions, Macromolecules. 35 (2002) 3213–3224. doi:10.1021/ma010858o.

[26] Y.M. Boiko, G. Guérin, V.A. Marikhin, R.E. Prud'homme, Healing of interfaces of amorphous and semi-crystalline poly(ethylene terephthalate) in the vicinity of the glass transition temperature, Polymer. 42 (2001) 8695–8702. doi:10.1016/S0032-3861(01)00406-2.

[27] K. Jud, H.H. Kausch, Load transfer through chain molecules after interpenetration at interfaces, Polym. Bull. 1 (1979) 697–707. doi:10.1007/BF00255445.

[28] M. Bousmina, H. Qiu, M. Grmela, J.E. Klemberg-Sapieha, Diffusion at polymer/polymer interfaces probed by rheological tools, Macromolecules. 31 (1998) 8273–8280. doi:10.1021/ma980562r.

[29] Y.H. Kim, R.P. Wool, A theory of healing at a polymer-polymer interface, Macromolecules. 16 (1983) 1115–1120. doi:10.1021/ma00241a013.

[30] M. Tirrell, Polymer Self-Diffusion in Entangled Systems, Rubber Chem. Technol. 57 (1984) 523–556. doi:10.5254/1.3536019.

[31] A. Lee, R.P. Wool, FT-IR study of orientation relaxation in uniaxially oriented monodisperse atactic polystyrenes, Macromolecules. 19 (1986) 1063–1068. doi:10.1021/ma00158a022.

[32] H. Watanabe, Viscoelasticity and dynamics of entangled polymers, Prog. Polym. Sci. 24 (1999) 1253–1403. doi:10.1016/S0079-6700(99)00029-5.

[33] S.F. Edwards, Dynamics of polymers in solution and melts, Polymer. 26 (1985) 163–168. doi:10.1016/0032-3861(85)90025-4.

[34] D.S. Pearson, G. Ver Strate, E. von Meerwall, F.C. Schilling, Viscosity and Self-Diffusion Coefficient of Linear Polyethylene, Macromolecules. 20 (1987) 1133–1141. doi:10.1021/ma00171a044.

[35] A.D. Godwin, Plasticizers, in: Appl. Plast. Eng. Handb., Elsevier, 2011: pp. 487–501. doi:10.1016/B978-1-4377-3514-7.10028-5.

[36] G. Wypych, ed., Handbook of Plasticizers, 2nd ed., Elsevier, Toronto, 2012. doi:10.1016/C2011-0-07408-2.

[37] E.H. Immergut, H.F. Mark, Principles of Plasticization, (1965) 1–26. doi:10.1021/ba-1965-0048.ch001.

[38] M.H. Khaliq, R. Gomes, C. Fernandes, J.M. Nóbrega, O.S. Carneiro, L.L. Ferrás, On the Use of High Viscosity Polymers in the Fused Filament FabricationProcess, Rapid Prototyp. J. 23 (2016) 727-735. doi:10.1108/RPJ-02-2016-0027.

[39] J.M. Chacón, M.A. Caminero, E.García-Plaza, P.J.Núñez, Additive manufacturing of PLA structures using fused deposition modelling: Effect of process parameters on mechanical properties and their optimal selection, (2017) 143-157. doi: 10.1016/j.matdes.2017.03.065

[40] S.F. Costa, F.M. Duarte, J.A. Covas, Estimation of filament temperature and adhesion development in fused deposition techniques, J. Mater. Process. Technol. 245 (2017) 167–179. doi:10.1016/j.jmatprotec.2017.02.026.

[41] J. Bartolai, T.W. Simpson, R. Xie, J. Bartolai, T.W. Simpson, Predicting strength of additively manufactured thermoplastic polymer parts produced using material extrusion, Rapid Prototyp. J. 24 (2018) 321–332. doi:10.1108/RPJ-02-2017-0026.

[42] C.S. Davis, K.B. Migler, Weld formation during material extrusion additive manufacturing, Soft Matter. 13 (2017) 6761–6769. doi:10.1039/c7sm00950j.

[43] ISO 1133, Plastics - Determination of the melt mass-flow rate (MFR) and melt volume-flow rate (MVR) of thermoplastics, ISO Standards.

[44] J.E. Seppala, K.D. Migler, Infrared thermography of welding zones produced by polymer extrusion additive manufacturing, Addit. Manuf. 12 (2016) 71–76. doi:10.1016/j.addma.2016.06.007.

[45] A.D. Amico, A.M. Peterson, An adaptable FEA simulation of material extrusion additive manufacturing heat transfer in 3D,

Addit. Manuf. 21 (2018) 422–430. doi:10.1016/j.addma.2018.02.021.

[46] S.M. Aharoni, Correlations between chain parameters and failure characteristics of polymers below their glass transition temperature, Macromolecules. 18 (1985) 2624–2630. doi:10.1021/ma00154a045.

[47] F. Yang, R. Pitchumani, Interlaminar contact development during thermoplastic fusion bonding, Polym. Eng. Sci. 42 (2002) 424–438. doi:10.1002/pen.10960.

[48] C. McIlroy, P.D. Olmsted, Disentanglement effects on welding behaviour of polymer melts during the fused- filament-fabrication method for additive manufacturing, Polymer. 123 (2017) 376–391. doi:10.1016/j.polymer.2017.06.051.

Figures and Tables

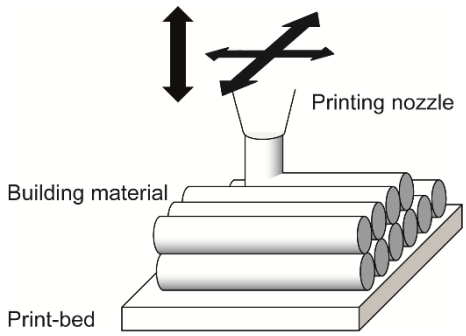

Fig. 1. Schematic representation of the FFF printing process: The movable printing nozzle feeds the heated building material onto the print-bed in a programmable pattern.

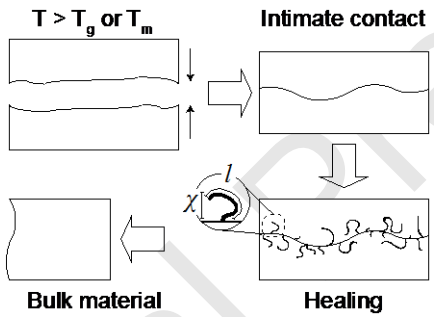

Fig. 2. Schematic representation of the healing process, illustrating the interpenetration depth χ, and the interpenetrated polymer chain length l (Illustration redrawn from reference 24).

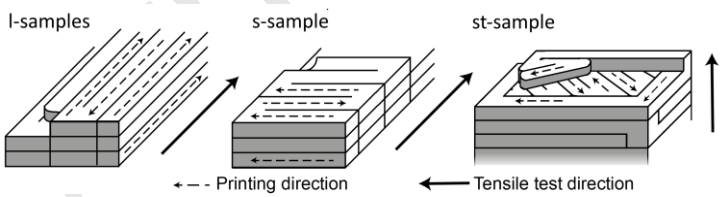

Fig. 3. Schematic representation of the l-sample (left), s-sample (middle) and st-sample (right) printing pattern for FFF-printed tensile test bars. The printing direction is indicated by dotted arrows and the tensile test direction is indicated by the bold arrow.

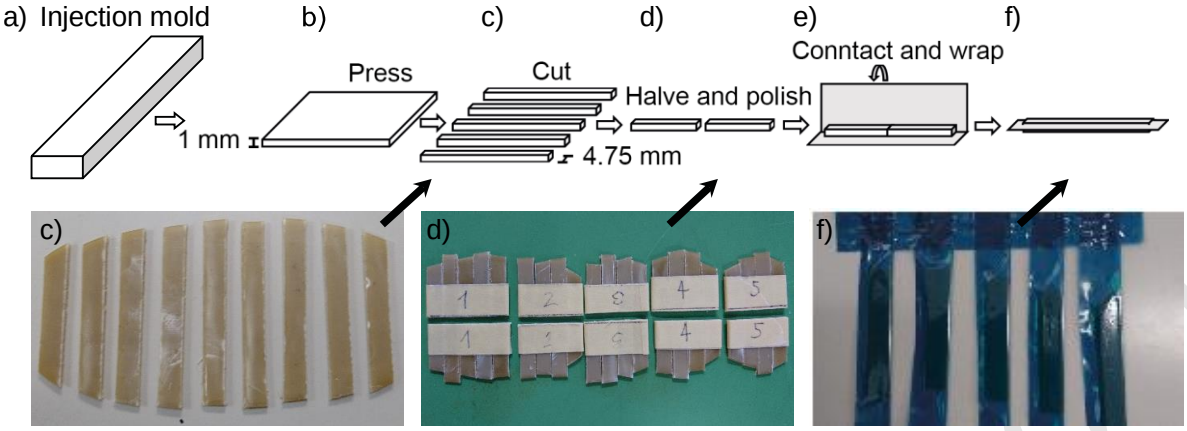

Fig. 4. Schematic representation and images of the sample preparation process for welding time tests, starting with a) the injection molded bar, which is b) being pressed into a 1 mm thick plate and c) cut into 4.75 mm wide strips. Those are in turn d) halved and polished and e) wrapped with adhesive tape to ensure alignment of the cut surface to f) obtain the wrapped sample before it is used in healing experiments.

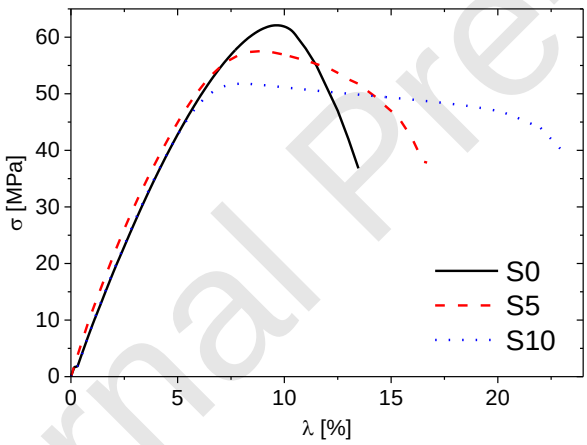

Fig. 5. Stress (σ) strain (λ) curves of injection molded samples. Average of five individual specimen.

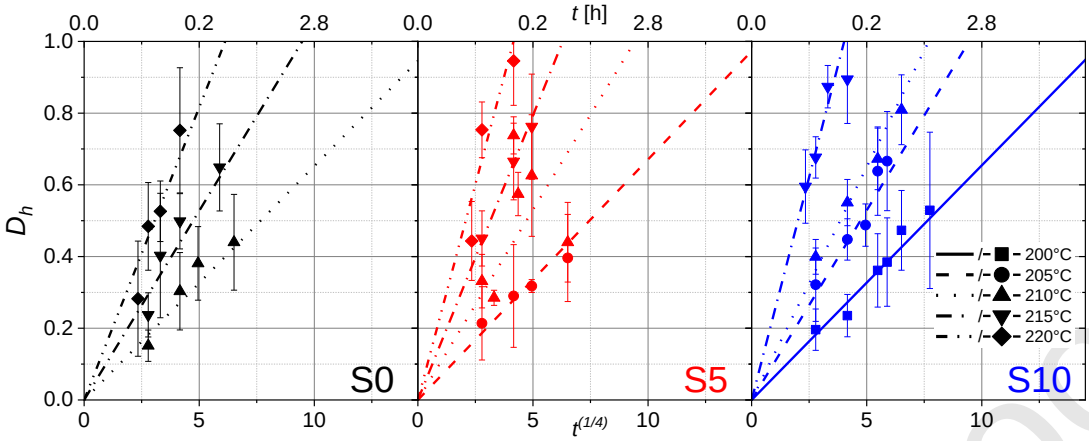

Fig. 6. Healing experiment results showing the degree of healing at different temperatures and times for S0, S5 and S10. The measured D_h values are and their standard deviation are described by the symbols, while the linear fits are shown as lines.

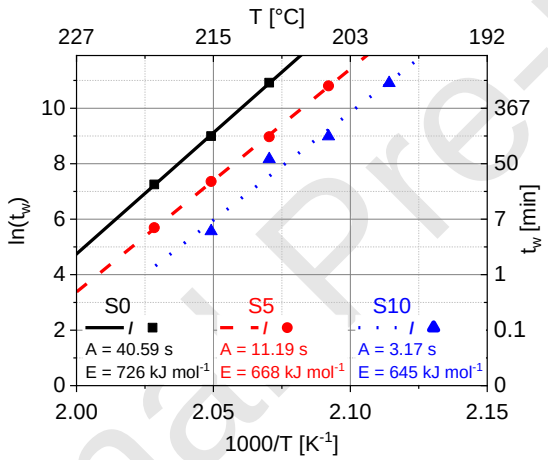

Fig. 7. Welding times t_w of S0, S5 and S10 (symbols), as well as the fit according to Equation 3 (lines) and the corresponding fit-parameters A and E, with a T_{ref} of 230°C.

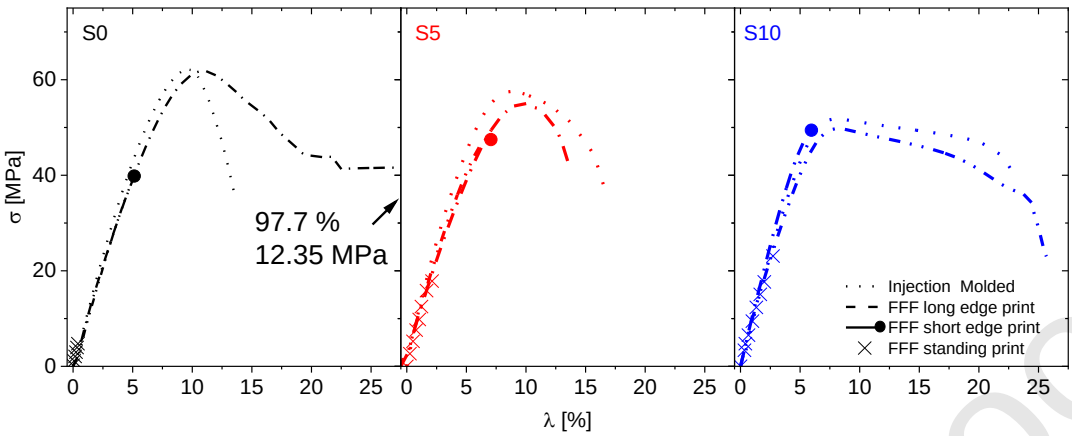

Fig. 8. Averaged Stress (σ) strain (λ) curves of injection molded samples (short dots), FFF l-samples (long dots) FFF s-samples (line) and FFF st-samples (crosses). The differences in tensile strength between injection molded and FFF s-samples are indicated.

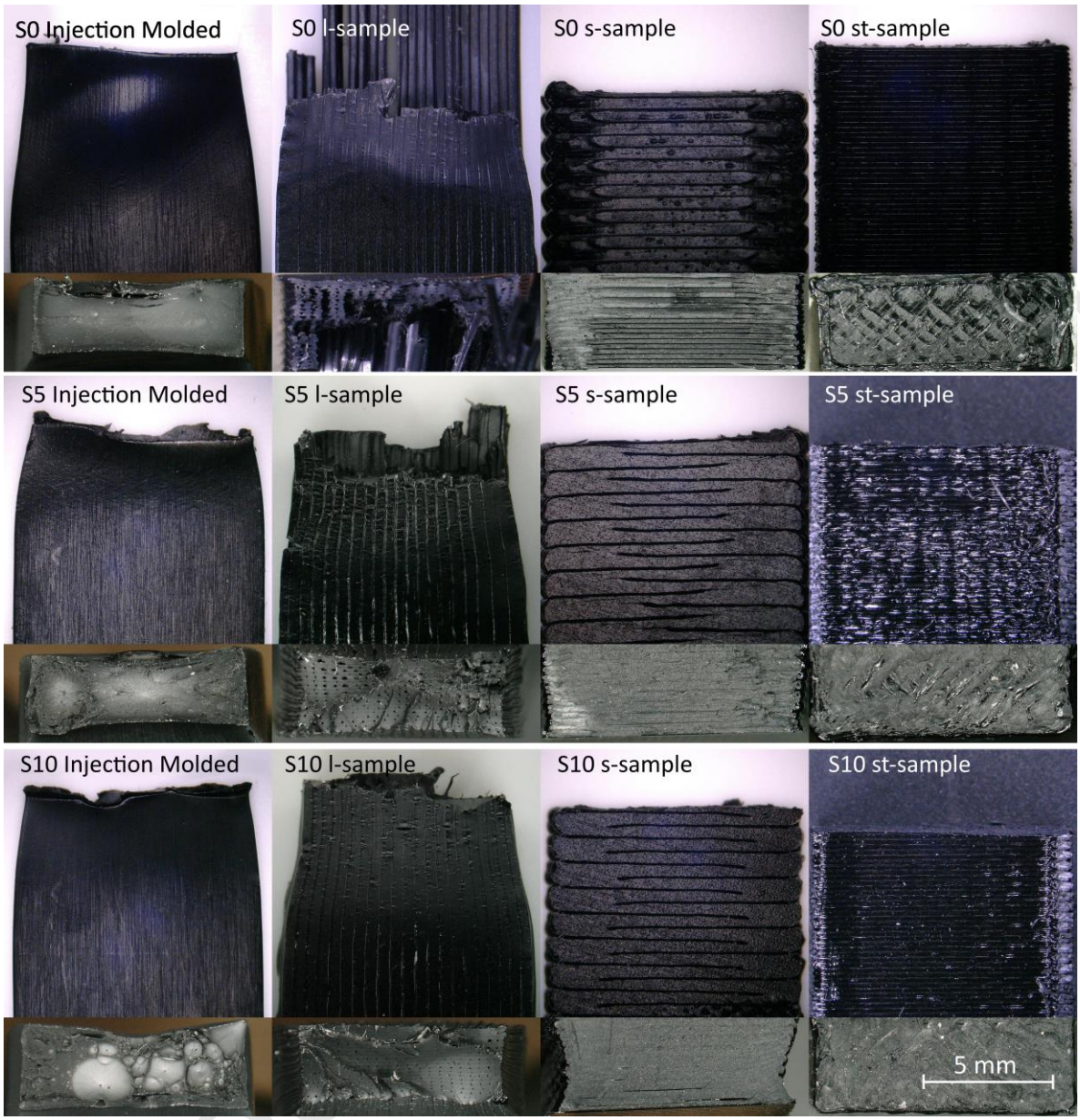

Fig. 9. Representative optical microscopy images of tensile test specimen failure surfaces, side view (upper images) and top view (lower images)

Table 1. Glass transition temperatures of the material S0, S5 and S10.

Sample	Tg [°C]
S0	107.9
S5	99.3
S10	91.8

Table 2. List of testing times *t* and temperatures T at which the three different materials (S0, S5, S10) were tested.

S0		S5		S10	
T [°C]	*t* [min]	*T* [°C]	*t* [min]	*T* [°C]	*t* [min]
210	1	205	1	200	1
210	5	205	5	200	5
210	10	205	10	200	15
210	30	205	30	200	20
215	1	215	1	200	30
215	2	215	5	200	60
215	5	215	10	205	1
215	20	220	0.5	205	5
220	0.5	220	1	205	10
220	1	220	5	205	15
220	2	-	-	205	20
220	5	-	-	210	1
-	-	-	-	210	5
-	-	-	-	210	15
-	-	-	-	210	30
-	-	-	-	215	0.5
-	-	-	-	215	1
-	-	-	-	215	2
-	-	-	-	215	5

Table 3. Temperatures during filament extrusion of the heating zones near the feeder (T_{feeder}), in the middle ($T_{fmiddle}$) and near the die (T_{die}), as well as the screw speed of the extruder and the belt speed of the filament winder.

Sample	T_{feeder} [°C]	T_{middle} [°C]	T_{die} [°C]	*Screw speed* [rpm]	*Belt speed* [rpm]
S0	225	230	235	1	0.5
S5	188	215	200	1	0.7
S10	205	215	198	1	0.7

Table 4. Summary of tensile test data: Young's modulus Y, Tensile strength σ, strain at maximum stress λ_m and strain at break λ_b of samples S0, S5 and S10 in their injection molded , l-sample, s-sample and st-sample form (∞, l, s and st as indices respectively).

Tensile Properties			S0	S5	S10
Young´s modulus	Y_∞	[MPa]	1061 ± 42	1080 ± 19	1134 ± 10
	Y_l	[MPa]	1139 ± 22	920 ± 44	1057 ± 18
	Y_s	[MPa]	1091 ± 37	989 ± 32	1038 ± 73
	Y_{st}	[MPa]	1118 ± 30	1011 ± 25	999 ± 99
Tensile strength	σ_∞	[MPa]	62.2 ± 1.2	57.5 ± 0.4	51.8 ± 0.8
	σ_l	[MPa]	61.9 ± 1.4	55.2 ± 1.1	49.8 ± 1.2
	σ_s	[MPa]	25.2 ± 4.9	47.5 ± 1.0	49.4 ± 2.5
	σ_{st}	[MPa]	4.7 ± 0.4	17.8 ± 3.4	23.1 ± 2.1
Strain at max σ	$\lambda_{m,\infty}$	[%]	9.8 ± 0.3	9.4 ± 0.1	8.0 ± 0.1
	$\lambda_{m,l}$	[%]	12.4 ± 0.3	10.5 ± 0.5	8.1 ± 0.3
	$\lambda_{m,s}$	[%]	3.2 ± 0.6	7.1 ± 0.3	6.0 ± 0.3
	$\lambda_{m,st}$	[%]	0.4 ± 0.03	2.1 ± 0.5	2.7 ± 0.4
Strain at break	$\lambda_{b,\infty}$	[%]	13.5 ± 2.6	19.7 ± 1.3	23.3 ± 1.4
	$\lambda_{b,l}$	[%]	96.6 ± 10.0	13.6 ± 2.2	25.7 ± 1.1
	$\lambda_{b,s}$	[%]	3.2 ± 0.6	7.1 ± 0.3	6.0 ± 0.3
	$\lambda_{b,st}$	[%]	0.4 ± 0.03	2.1 ± 0.5	2.7 ± 0.4

Table 5. List of welding times t_w at different temperatures T, which were tested.

T [°C]	t_w [min]		
	S0	S5	S10
200	-	-	909.4
205	-	822.7	133.0
210	920.6	131.5	58.5
215	134.3	26.2	4.4
220	23.5	5.0	-

Table 6. Summary of healing results of samples S0, S5 and S10: Rate constant A, activation energy E, MFI value and degrees of healing of s-, l- and st-samples $D_{h,s} = \sigma_s / \sigma_\infty$, and $D_{h,l}$ and $D_{h,st}$ respectively.

Sample	Healing experiment		Flow properties	Interface adhesion		
	A [s]	E [kJ mol^{-1}]	MFI [g (10 min)$^{-1}$]	$D_{h,l}$ [%]	$D_{h,s}$ [%]	$D_{h,st}$ [%]
S0	726	40.6	4.3	99	41	8
S5	688	11.2	9.5	96	83	31
S10	688	0.5	21.6	96	95	45

Table 6. $D_{h,s}$ as calculated by the method of Costa et al.[38]

Sample	$D_{h,calc}$ [%]
S0	81
S5	92
S10	99